Phonon spectroscopy of the electron-hole liquid in germanium

W. Dietsche,* S. J. Kirch, and J. P. Wolfe
Physics Department and Materials Research Laboratory, University of Illinois at Urbana-Champaign, Urbana, Illinois 61801
(Received 10 November 1981)

The absorption of phonons by the electron-hole liquid (EHL) in semiconductors has proven to be the principal process causing macroscopic transport of droplets of this Fermi fluid. A characterization of the phonon absorption for frequencies of several hundred gigahertz promises to elucidate this "phonon wind" transport mechanism as well as test the basic theory of deformation potential scattering within a degenerate Fermi liquid. Central predictions of this theory are an absorption rate which increases linearly with frequency at low frequencies and a transparency for phonon wave vectors greater than $2k_F$, where k_F is the Fermi wave vector of the liquid. We have adapted the standard deformation potential theory to the case in which the phonon energies are comparable to the Fermi energy and have calculated the frequency and angle dependences of the phonon absorption by electron-hole liquid in Ge. The sharpness and position of the $2k_F$ cutoffs depend upon propagation direction and phonon polarization. Using the method of tunnel-junction phonon spectroscopy, we have measured the absorption of monochromatic phonons by electron-hole liquid over the frequency range 150–500 GHz. We concentrated on longitudinal phonons with $\vec{q}\|\langle 111\rangle$, the long axis of an electron energy ellipsoid. By applying an appropriate uniaxial stress to the crystal we were able to vary the population of this valley, thereby continuously "tuning" the predicted $2k_F$ cutoff over a factor of about 4. The resulting absorption spectra agreed with theoretical predictions, displaying for the first time the $2k_F$ cutoff for this Fermi liquid. To determine the absolute phonon absorption length in EHL, we used a luminescence-imaging method to calibrate the volume of liquid in the phonon path. Our measured deformation potential is smaller than that obtained for free electrons in Ge via cyclotron resonance. We interpret this reduction in electron-phonon interaction strength as due to screening within the electron-hole liquid. This interpretation is consistent with a recent theoretical calculation.

I. INTRODUCTION

At low temperatures, photoexcited carriers in a semiconductor can condense into a Fermi fluid known as the electron-hole liquid (EHL). Many properties of this phase have been studied since its discovery in 1967.[1] A large majority of the experiments have been conducted in Ge, where the indirect band structure permits a very stable liquid phase with a lifetime of many microseconds. It has been shown both experimentally and theoretically that at low temperatures the liquid density in Ge is 2.3×10^{17} pairs/cm^3, a value which is fixed by the band structure and many-body energetics. An increase in the excitation level increases the total volume of the liquid, not its density. This density corresponds to an electron Fermi energy, $E_F^e=2.53$ meV. Since the electron valleys in Ge are ellipsoids with their long axes along the $\langle 111\rangle$ directions, the Fermi wave vector is anisotropic with a maximum value of $k_F(\langle 111\rangle)=3.23\times10^6$ cm^{-1}.

In recent years experiments have concentrated on the macroscopic transport of the EHL. Generally, the liquid is formed as a diffuse collection of droplets, each a few micrometers in diameter, dispersed throughout a cloud with a filling factor of about 1%. Even though the carriers are typically produced by focused surface excitation, the size of the cloud can be surprisingly large, up to several millimeters across, with a volume proportional to the excitation level. This observation led Keldysh[2] to postulate, in 1976, that the electron-hole droplets are driven into the crystal, from the surface where they are created, by a "phonon wind." A number of varied experiments by several research groups[3–9] have since provided strong support for this hypothesis.

The basic idea of the phonon-wind transport mechanism is contained in Fig. 1. This figure

shows a cross section of one of the ellipsoidal electron valleys in $\vec{k}$ space. A phonon with wave vector $\vec{q}$ can be absorbed and cause an electron transition from $\vec{k}_1$ to $\vec{k}_2$. The momentum $\vec{q}=\vec{k}_2-\vec{k}_1$ gained by the electron will be quickly ($<10^{-9}$ sec) distributed to all the other electrons by electron-electron interaction, giving a net momentum to the droplet as a whole. Similar arguments also apply to the holes.

It is clear from the schematics in Fig. 1 that the requirements of energy and momentum conservation will severely restrict the possible transitions. In particular, phonons with $\vec{q}$ vector much larger than $2k_F$ will not be absorbed, leading to a $2k_F$ cutoff in the absorption. This type of cutoff has been previously considered in other metallic systems.[10] However, for the EHL this cutoff will not necessarily be very sharp, because the sound velocity of the phonons is comparable to the Fermi velocity. This is equivalent to saying that the energy $\hbar\omega$ of a phonon with $q=2k_F$ is a fair fraction of the Fermi energy E_F^e, as illustrated in Fig. 1(b).

A natural method for studying this electron-phonon interaction is to observe the absorption of high-frequency phonons by EHL. The first experiments of this type were performed by Hensel and Dynes,[4] who used heat pulses as the phonon source. These experiments verified the prediction that longitudinal phonons are more strongly absorbed by EHL than transverse phonons. By varying the temperature of their heat source, these authors concluded that the phonon absorption was reduced for higher-frequency phonons. No quantitative determination of the absorption spectrum was attempted, however, because of the extremely broad (Planck-type) spectrum of the phonon source.

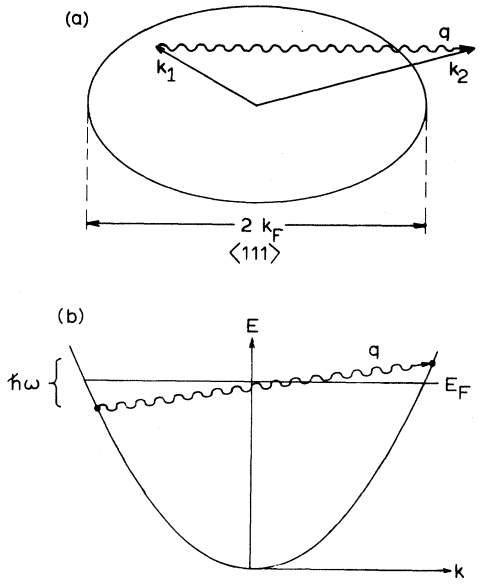

FIG. 1. Absorption of a phonon by the EHL. The electron is scattered from $\vec{k}_1$ to $\vec{k}_2$ by a phonon of wave vector $\vec{q}$. (a) A cross section of the Fermi ellipsoid. (b) The parabolic electron valley.

In this article, we apply the relatively new technique of tunnel-junction phonon spectroscopy[11,12] to study the interactions of high-frequency phonons with the EHL. In this method, monochromatic phonons are generated and detected by superconducting tunnel junctions. By passing these phonons through a cloud of electron-hole droplets, we have measured the frequency dependence of the phonon absorption by EHL. Simultaneously, we have measured the spatial distribution of infrared recombination luminescence from EHL to calibrate the cloud density. Combining these experiments, we have made a measurement of the absolute phonon absorption strength, and thus the phonon deformation potential. By stressing the crystal we have modified the band structure of the EHL and have observed the predicted $2k_F$ cutoff over a wide range.

In Sec. II of this paper we will present theoretical calculations of the phonon absorption by a Fermi liquid. Although the parameters used are those of an EHL in Ge, the results will be applicable to other anisotropic degenerate systems, e.g., highly doped semiconductors and semimetals. In Sec. III we will describe the experiments, including the phonon spectroscopy method, the absorption measurements, and the determination of the cloud density. In Sec. IV we will discuss our results.

II. THEORETICAL BACKGROUND

The theory of absorption and emission of phonons by carriers in a semiconductor was developed originally by Bardeen and Shockley.[13] Herring and Vogt[14] generalized this theory for the case of ellipsoidal constant-energy surfaces. The basic idea is that the scattering matrix element for a phonon of wave vector $\vec{q}$ is given by the energy shift of the electron valleys due to a *static* strain with the same strain components as the phonon. This energy shift is called the deformation potential.

In Ge, the electron valleys are along the ⟨111⟩ axes and the deformation potentials for a given phonon mode (longitudinal or transverse) and propagation direction can be described in terms of two

deformation potential constants, Ξ_d and Ξ_u. The absorption of a phonon of mode α and wave number q is described by the matrix element,

$$|M(q,\alpha)|^2 = N_q \sum_{rs} \Xi_r \Xi_s f_r f_s \hbar\omega_q / 2V\rho v_\alpha^2 , \quad (1)$$

where N_q is the phonon occupation number.

The deformation potentials are

$$\Xi_r = \Xi_d + \Xi_u/3 \quad \text{for } r = 1,2,3$$

and

$$\Xi_r = \Xi_u/3 \quad \text{for } r = 4,5,6 .$$

f_r are the "strain polarization factors" for the mode α and direction $\vec{q}$, v_α is the phonon phase velocity, ρ is the crystal density, and V is the crystal volume.

The values of Ξ_d and Ξ_u have been determined[15] for single electrons in Ge from cyclotron resonance under uniaxial stress to be -12.3 and 19.3 eV, respectively. Recently, Markiewicz[16] predicted that in EHL, Ξ_d is reduced to -7.1 eV due to screening effects. We will use the latter value in our calculation.

The quantity

$$\Xi_\alpha^2 = \sum_{rs} \Xi_r \Xi_s f_r f_s$$

is the square of the deformation potential for the phonon mode α. We have calculated Ξ_α^2 for phonons in the (110) plane, and the corresponding plot is shown in Fig. 2. The deformation potentials are highly anisotropic and quite different for the three phonon modes. Note that for a given direction in the (110) plane one transverse mode always has a zero deformation potential.

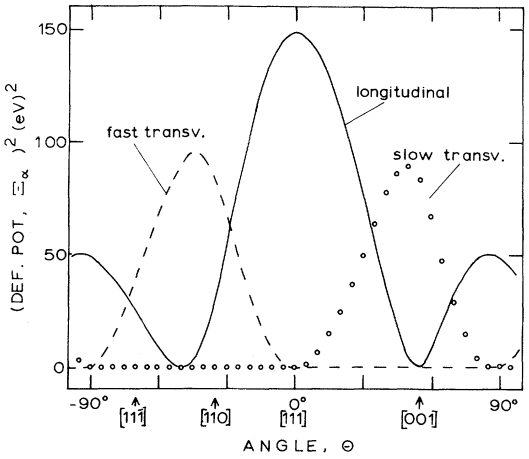

FIG. 2. Calculated total deformation potential Ξ_α^2 for phonon wave vector $\vec{q}$ in the (110) plane as a function of angle θ from the [111] direction. LA, solid line; fast TA, dashed line; slow TA, dotted line.

The rate of change in the phonon occupation, N_q, due to phonon absorption by electrons is given by

$$\frac{\partial N_q}{\partial t} = -\frac{2\pi}{\hbar} \sum_{\vec{k}_1} |M(q,\alpha)|^2 \delta(\epsilon_1 + \hbar\omega_q - \epsilon_2) \times f(\epsilon_1)[1-f(\epsilon_2)] , \quad (2)$$

where the summation is over all initial electron states $\vec{k}_1$. In this expression, ϵ_1 is the energy of the initial electron state, ϵ_2 is the energy of the final state, and $f(\epsilon)$ are the Fermi factors. The emission of phonons is negligible because the temperature is very low. An evaluation of Eq. (2) for the case of ellipsoidal energy surfaces can be found in Conwell's monograph.[17] We generalized the result slightly to account for the nonzero sound velocity and Fermi statistics. It follows that the inverse scattering time for the mode α is given by

$$\frac{1}{\tau_\alpha} = \frac{\Xi_\alpha^2 m_0}{4\pi^2\hbar^2\rho v_\alpha} \left[\frac{m_\perp^2 m_{||}}{m_0^3}\right]^{1/2} \frac{q}{q^*} \times \int_{\phi^*=0}^{2\pi} \int_{k_0^*}^{\infty} dk^* k^* f(\epsilon_1)[1-f(\epsilon_2)] \quad (3)$$

with

$$k_0^* = \left| \frac{q^*}{2} - \frac{m_0 v_\alpha}{\hbar} \frac{q}{q^*} \right| , \quad (3a)$$

where the * denotes variables in the coordinate system in which the Fermi surface is a sphere, m_0 is the electron mass, $m_\perp$ and $m_{||}$ are the effective masses of the electrons, and

$$q^* = q \left[\frac{m_0}{m_\perp} \sin^2\theta + \frac{m_0}{m_{||}} \cos^2\theta \right]^{1/2} \quad (3b)$$

with θ the angle between $\vec{q}$ and the long axis of the ellipsoid ($\langle 111 \rangle$). Equation (3) is easily evaluated numerically. For the effective masses we use the renormalized values[18,19] $m_\perp^{\rm EHL} = 1.15 m_\perp$ and $m_{||}^{\rm EHL} = 1.0 m_{||}$, where $m_\perp = 0.82 m_0$, $m_{||} = 1.56 m_0$ for free electrons.

The resulting inverse lifetime of longitudinal phonons traveling in the [111] direction is plotted as function of phonon frequency in Fig. 3. The different curves correspond to different (hypothetical) Fermi energies. Under zero stress the Fermi

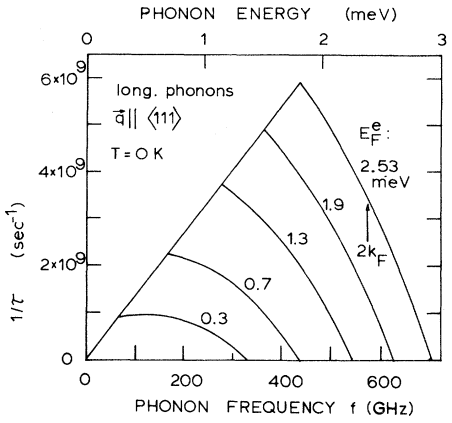

FIG. 3. Theoretical inverse lifetime of LA phonons in EHL in Ge with $\vec{q}||[111]$ as a function of frequency at $T=0$ K. Each curve is labeled with its corresponding Fermi energy E_F^e. The arrow indicates $\hbar(2k_F)v_s/2\pi$ for $E_F^e=2.53$ MeV, which is the zero-stress EHL value.

energy of the electrons in the EHL is 2.53 meV. It is notable that the $2k_F$ cutoff is relatively broad and is even broader than the linearly increasing region for lower Fermi energies, as shown. This is because at these rather small Fermi energies, $E_F \approx 3$ meV, the kinetic energy of an electron is not much larger than the phonon energy $\hbar\omega=\hbar v_s(2k_F)$. It is only when the Fermi velocity is much larger than the sound velocity that the cutoff is relatively sharp. In these graphs $v_s(2k_F)/2\pi$ occurs at the middle of the downward sloping region and is denoted by an arrow for $E_F^e=2.53$ meV.

In Fig. 4 we plot the inverse lifetime as the angle θ of the phonon wave vector with respect to the $\langle 111\rangle$ direction is varied. A large anisotropy is indeed observed, with $\vec{k}||\langle 111\rangle$ the direction of strongest absorption. The cutoff becomes sharper as θ increases, as one would expect for directions in which the effective masses are smaller and hence the Fermi velocities are larger.

Results for transverse phonons are shown in Fig. 5 for the two directions [110] and [001]. Notice that the absorption scale is much smaller than that for LA phonons. Also, the cutoff for TA phonons is sharper due to their smaller sound velocity. Comparing the different modes and directions shows that the absorption is by far the strongest for LA phonons in the $\langle 111\rangle$ direction.

So far the calculations have assumed that the temperature of the carriers is zero. The effect of an elevated temperature for two particular phonon modes is shown in Fig. 6. While the shape of the cutoff is only slightly affected by a temperature rise, the absorption strength at low frequency is increased, particularly for the transverse phonons. Our experiments concentrate on the longitudinal phonons along the $\langle 111\rangle$ direction, with the EHL temperature of the order of 1.5 K, implying that the temperature effects will be negligible.

In reality, phonons can be scattered by electrons in any one of the four valleys. If the phonon direction is [111], one valley will be crossed at $\theta=0°$ and the other three valleys will be crossed at an angle of $\theta=70.5°$. At this angle, the absorption strength is too weak to be visible on the scale of Fig. 3 or Fig. 4.

Phonons can also be absorbed by the holes. If this process is important it will be easy to distinguish, at least, in the [111] direction. In particular, we estimate the cutoff due to the holes to be at a much lower frequency (250 GHz) because of the smaller effective mass. This cutoff should be quite distinct from the one near 550 GHz due to the

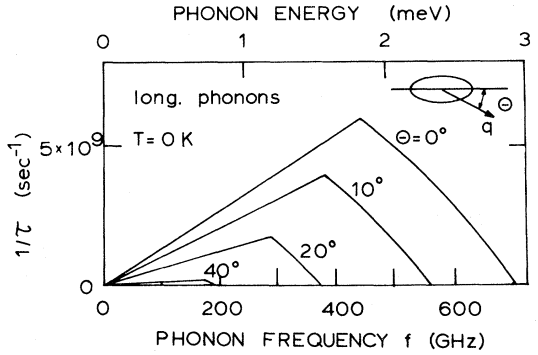

FIG. 4. Theoretical inverse lifetime of LA phonons in EHL in Ge as a function of frequency at $T=0$ for different angles θ in the (110) plane, from the [111] direction.

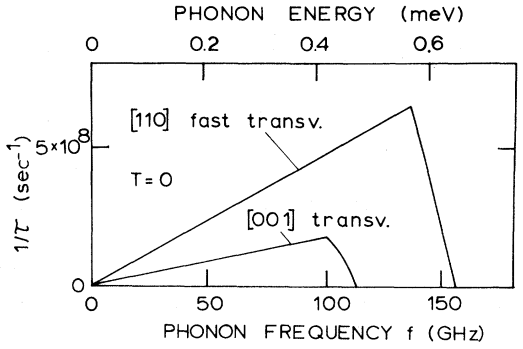

FIG. 5. Theoretical inverse lifetime of TA phonons with $\vec{q}||[110]$ (fast TA) and $\vec{q}||[001]$ (slow TA) in EHL at $T=0$ K as a function of frequency.

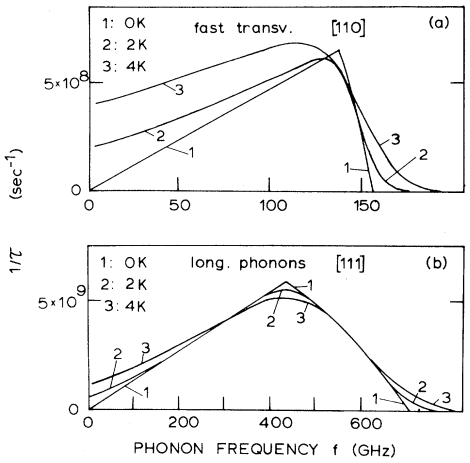

FIG. 6. Effect of finite temperature on the inverse lifetime in EHL of (a) TA phonons and (b) LA phonons. Notice the difference in scales.

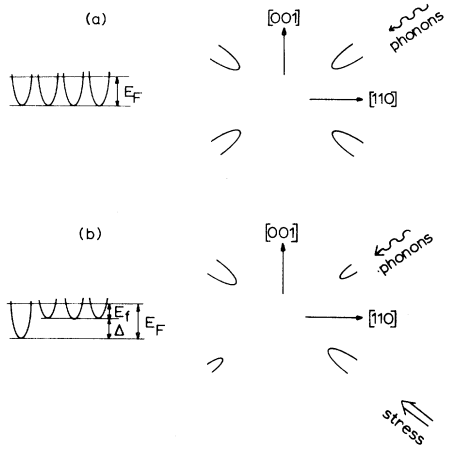

FIG. 7. Effect of stress on the electron valleys in EHL. (a) Unstressed Fermi surfaces with all valleys equally populated; (b) uniaxial $[11\bar{1}]$ stress. One valley shifts down by Δ, causing the other three to depopulate.

electrons.

As we have seen, phonons propagating in the [111] direction are mainly absorbed by electrons in the [111] valley. Generally, all four valleys are equally populated in the electron-hole liquid. However, there is a systematic method for changing the relative populations of these four valleys: the application of uniaxial stress. This provides a unique opportunity to greatly modify the phonon absorption spectrum.

For example, stress along the $[11\bar{1}]$ direction lowers the energy of the $[11\bar{1}]$ valley, while raising the energy of the [111], $[\bar{1}11]$, and $[1\bar{1}1]$ valleys. With only about 30 MPa (3 kgf/mm^2) it is possible to split these valleys by about the zero-stress Fermi energy, causing the upper three valleys to become completely depopulated. This fourfold reduction in the density of states reduces the equilibrium density of the EHL by about a factor of 3, although the Fermi energy is changed by only about 20% at 30 MPa. The ground-state properties of the EHL in Ge under uniaxial stress have been studied by several groups.[20–23]

From the point of view of phonon absorption, stress can have a dramatic effect, allowing us to "tune" the $2k_F$ cutoff *along certain directions* by a factor of about 4. Figure 7 illustrates this idea. This is a cross section of the valleys in the (110) plane in $\vec{k}$ space. Under zero stress all valleys are filled up to the same Fermi momentum $\vec{k}_F \| \langle 111 \rangle$ as given by E_F [Fig. 7(a)]. Uniaxial stress along the $[11\bar{1}]$ direction [Fig. 7(b)] leads to a splitting Δ of the bands. Three valleys, including the one along [111], are raised in energy. These upper valleys are filled only up to $E_f = E_F - \Delta$. Values of E_F and Δ as a function of stress have been previously measured.[21,22] Thus the expected cutoff frequency for the partially populated [111] valley, as a function of stress, is easily calculated.

III. EXPERIMENTS AND RESULTS

A. Phonon generation and detection

The calculations in Sec. II showed that the $2k_F$ cutoff is expected to occur at phonon frequencies on the order of a few hundred gigahertz. In this frequency range, superconducting tunnel junctions are presently the only source of monochromatic and frequency-tunable phonons.[24] A detailed description of this technique can be found in the pioneering papers of Kinder.[11]

Here we briefly summarize those aspects of tunnel-junction spectroscopy important to our experiments. As shown schematically in Fig. 8, if a voltage V is applied across a superconductor-insulator-superconductor junction, the tunneling electrons gain additional kinetic energy. In a process similar to bremsstrahlung generation in an x-ray tube, this electron energy is converted to high-energy phonons with a frequency spectrum dependent on V as in Fig. 8(c). A small modulation of V primarily changes the number of phonons near the cutoff frequency, $eV - 2\Delta_G$. Thus the modulated phonon spectrum is nearly monochromatic with a spectral width limited mainly by the modulation amplitude. In our case, this spectral resolu-

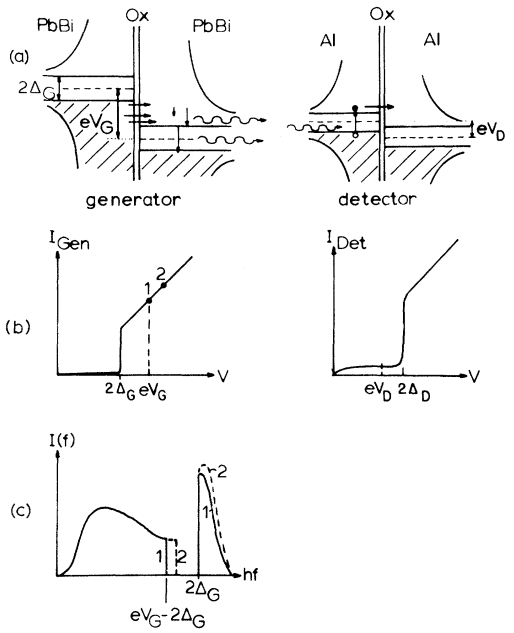

FIG. 8. Schematic of the phonon spectroscopy technique used here. (a) Quasiparticle densities of states in a generator and a detector junction (semiconductor picture). The generator is biased at a voltage $V_G > 2\Delta_G/e$. Quasiparticles can tunnel and gain energy in the process. The excess energy is emitted as phonons in relaxation (or bremsstrahlung) and recombination processes. The detector bias V_D is less than $2\Delta_D/e$. Incident phonons create quasiparticles which can tunnel and increase the tunneling current. The phonon energy must, of course, exceed $2\Delta_D$ to be detected. (b) I-V characteristics of generator and detector. V_G and V_D are the respective bias voltages. During pulse modulation the generator bias moves from 1 to 2. (c) Generated phonon spectrum for the generator bias V_G (curve 1) consisting of a low-frequency bremsstrahlung and a high-frequency recombination part. Modulation causes a shift in the edge at $eV-2\Delta_G$ and an increase in the peak near $2\Delta_G$ (curve 2).

tion was about 50 GHz. We used pulse modulation throughout, which allowed time-of-flight separation of longitudinal and transverse phonons.[25]

In principle, the nonmonochromatic part consists of phonons with a frequency close to $2\Delta_G$, known as "2Δ phonons." In practice, however, the signal also seems to contain products of inelastic decay processes in the generator junction films. These products and the 2Δ phonons produce a background of phonons which are modulated together with the monochromatic signal.

In our experiment, the generator junction was made of films of $Pb_{0.85}Bi_{0.15}$ alloy, directly evaporated on the Ge crystal surface. This alloy has a large superconducting gap ($2\Delta_G = 3.15$ meV) which permits a generation of phonons up to 770 GHz ($2\Delta_G/h$). The use of these junctions in phonon spectroscopy was previously demonstrated by Kinder and Dietsche.[26] Although 770-GHz phonons can be emitted by the generator, isotope scattering prevented phonons with frequencies above 500 GHz from propagating across our crystals. The effect of isotope scattering is discussed in the Appendix.

For the detectors we used superconducting tunnel junctions[27] made of granular Al films. Each junction detected phonons with frequencies above its energy gap, approximately 150 GHz, with a sensitivity which was dependent on its temperature. Although the crystal was immersed in a superfluid He bath at 1.3 K, it was found that both photoexcitation and variations in the dc phonon emission of the generator caused changes in the detector bias. To overcome this difficulty, an additional resistive heater was placed in the He bath to produce a comparable change in detector bias and an active feedback circuit was used to keep the detector sensitivity constant.[11]

B. Samples and apparatus

Our high-purity Ge samples ($N_A + N_D \leq 10^{12}$ cm^{-3}) were grown by Haller and Hansen of the Lawrence Berkeley Laboratory. In our initial zero-stress experiments we used a sample with dimensions $4\times10\times10$ mm^3, with the junctions placed on the large faces. Stress experiments were done with a sample of dimensions $3.4\times2.9\times10$ mm^3. Variable uniaxial stress was applied along the $[11\bar{1}]$ direction, which was the long axis of this sample. The experimental arrangement is shown in Fig. 9(a). Generator and detector were placed on opposing surfaces so that the path of the detected phonons was along the desired crystal direction. We placed the junctions within 0.5 mm of the excitation surface in order to maximize the phonon absorption by the droplet cloud. The phonon focusing properties of Ge (Ref. 28) helped to avoid any interference due to reflections from the excitation surface.

Electron-hole liquid was created in the phonon path using a cw Nd:YAG (yttrium aluminum garnet) laser ($\lambda = 1.06$ μm). For this type of excitation, EHL droplets are produced at the surface and are pushed into the crystal by a phonon wind,[9] forming a diffuse cloud of small droplets with

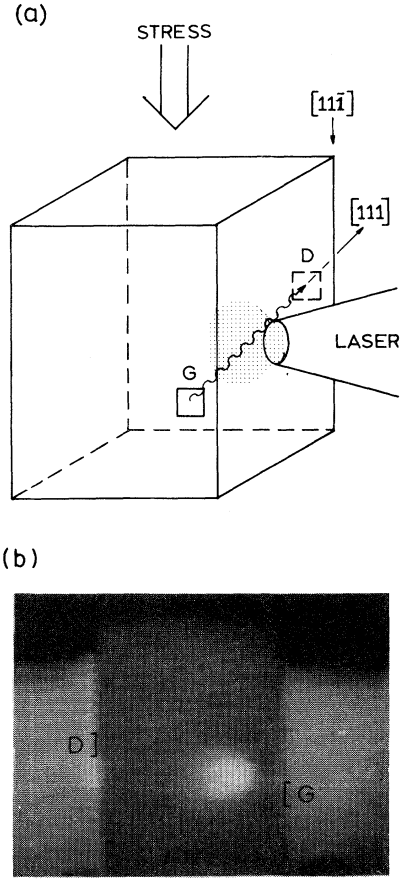

FIG. 9. (a) Schematic of the stressed crystal orientation. The generator (G) and detector (D) are on opposite faces of the crystal approximately 0.5 mm from one edge placed so that the phonons propagate in the desired direction [111]. A slightly defocused laser beam (spot size $\simeq$0.5 mm) produced a cloud of droplets which intercepted the phonon path. Stress was applied in the [11$\bar{1}$] direction corresponding to Fig. 7(b). (b) Photograph of an infrared vidicon image showing the actual crystal. The view is toward the laser. The bright spot is luminescence from the EHL cloud. The positions of the generator and detector are shown.

about a 1% filling factor. The cloud radius (not the EHL density in each droplet) increases with excitation level. For our absorbed power of 10 to 20 mW a cloud with a radius of 1 to 2 mm was produced. The cloud position, size, and density were monitored by detecting its recombination luminescence at $\lambda=1.75$ μm with an infrared-sensitive imaging system.[9] The spatial distribution of the cloud was determined with a resolution of 0.15 mm.

To stress the crystal, a spring-loaded plunger pressed the sample between two indium-padded, stainless-steel blocks. A ball bearing contacted one of the blocks in order to minimize inhomogeneous shear strains in the crystal. The magnitude of the crystal stress as well as its homogeneity was determined directly from the spectral shift of the exciton luminescence at 3.0 K (Ref. 29). The inhomogeneity over the phonon path was found to be less than 10%.

Figure 9(b) shows a picture of the stress arrangement taken with the imaging system. The viewer is looking into the laser beam. The bright region is luminescent light from the EHL cloud. The position of the junctions are marked G (generator) and D (detector).

C. Phonon absorption measurements

The ballistic propagation of the high-frequency phonons is seen in Fig. 10. At $t=0$, a 150-nsec modulation pulse is applied to the generator junction, producing phonon pulses which propagate at their sound velocity and are observed at the detector junction. LA and TA phonons are easily distinguished by their differing times of flight.

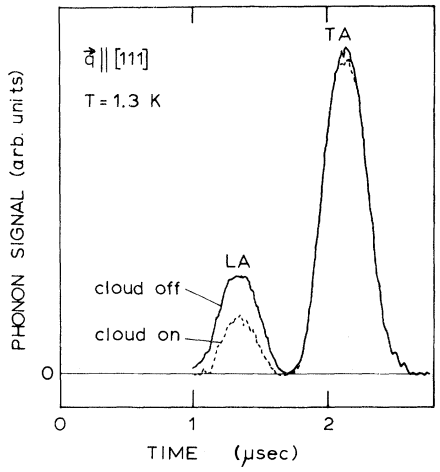

FIG. 10. Phonon signal as a function of time after the modulation pulse at the generator. The LA and TA peaks are easily distinguished by their differing velocities for $\vec{q}$||[111]. The solid line is with no optical excitation and the dashed line shows the effect of interposing an EHL cloud.

The phonon signals were significantly changed when a cloud of droplets was present. The solid line was taken without an EHL cloud and the dotted line with a cloud in the phonon beam. Comparison of the two traces shows that the presence of the EHL cloud reduced the LA signal by about 45% while the TA signal is reduced by less than 3%. This result agrees very well with that of Hensel and Dynes, who used resistively generated heat pulses.[4]

Traces of the LA-phonon intensities as functions of frequency are shown in Fig. 11. These traces were highly reproducible and contain features typical of all the traces taken. At 150 GHz (which we label $F1$) the monochromatic phonon energy exceeds the detector threshold, which results in a distinct increase of the signal above the background signal. An additional increase in signal at about 300 GHz is due to an increased detector sensitivity caused by multiple reemission and reabsorption processes in the detector. At 400 GHz, the monochromatic part of the signal begins to decrease due to isotope scattering, as discussed in the Appendix. Above 520 GHz (which we label $F2$) only background phonons are detected.

For a quantitative treatment of the phonon absorption by the EHL, it is necessary to subtract the background due to nonmonochromatic phonons. Since the exact ratio between background and monochromatic phonons has not yet been determined for this type of generator we used the following approximation: We know that no monochromatic phonons are detected below $F1$ due to the detection threshold and above $F2$ due to the isotope scattering. Connecting the intensities at $F1$ and $F2$ with a straight line [the curve labeled (1) in Fig. 11] gives a possible choice of background. From earlier spectroscopic work with $Pb_{0.85}Bi_{0.15}$ generators, a background more like line (2) appears equally possible.[26,30] We will analyze our data using both backgrounds separately and will include the resulting differences in the final error estimate.

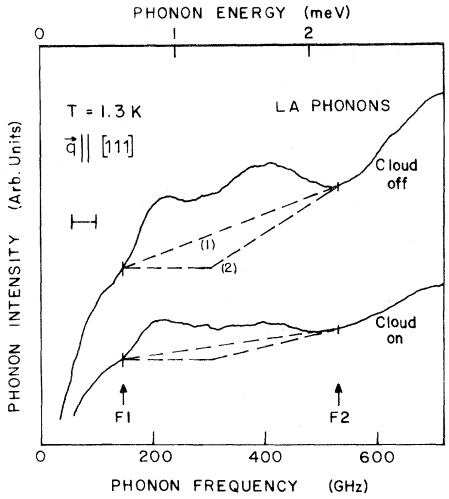

FIG. 11. Phonon spectra showing the frequency dependence of the absorption of LA phonons $\vec{q}||[111]$. $F1$ is the detector threshold and $F2$ the isotope scattering cut on (see text). (1) and (2) are two choices for background.

The object of these experiments is to determine as a function of frequency the mean free path, l, of a phonon traveling through pure electron-hole liquid. We assume that the monochromatic phonon intensity I at the detector is reduced according ing to the relation,

$$I = I_0 \exp(-d/l) , \tag{4}$$

where I_0 is the monochromatic phonon intensity measured without the cloud and d is the total path length of the phonons through the electron-hole liquid. This expression assumes, of course, that the electron-hole droplets block the entire cross section of the detector beam; otherwise a fraction of the phonon intensity will be independent of d. This issue will be discussed later.

One can readily see from the data of Fig. 11 that the higher-frequency phonons are attenuated more than the lower-frequency phonons. The ratio I/I_0, as a function of frequency, is determined from the two traces giving the frequency dependence of d/l which is plotted in Fig. 12(a). The ends of the error bars indicate the differing results obtained by using the two alternative backgrounds. As seen in this plot the final result is not especially sensitive to the choice of background.

The data in Fig. 12(a) shows a linear increase in d/l with phonon frequency as expected from the theory. The phonon frequency is related to the phonon wave vector by the relation $\omega = v_s k$, where $v_s = 5.6 \times 10^5$ cm/sec for LA phonons in the $\langle 111 \rangle$ direction. The dashed line is a theoretical fit using the product of d and Ξ_a^2 as a parameter. Unfortunately, the frequency range of the $2k_F$ cutoff coincides with the onset of the isotope scattering. Therefore, we could not directly observe the $2k_F$ cutoff in this unstressed crystal.

No clear indication of a phonon absorption by the holes is visible in Fig. 12(a). The holes should contribute a small absorption below about 250 GHz; however, this effect is expected to be much smaller than the electron absorption.

In addition to the [111]-propagation experiments

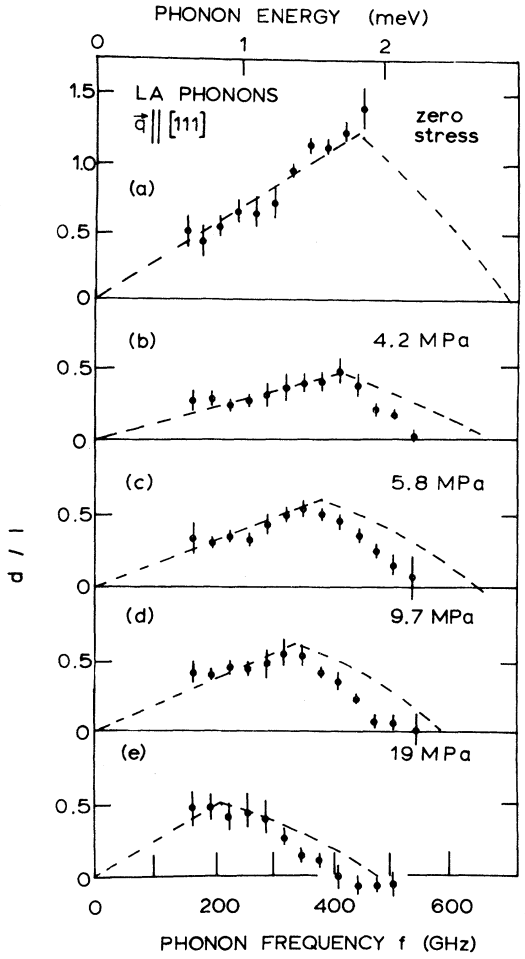

FIG. 12. Plots of our measured $-\ln(I/I_0)$ vs frequency for various stresses. This equals d/l if all phonons intercept EHL (see Sec. III E). Dots are the data points; the error bars indicate the effect of the different backgrounds. The dashed lines are fits to the theory using $\Xi_\alpha^2 d$ as a single parameter.

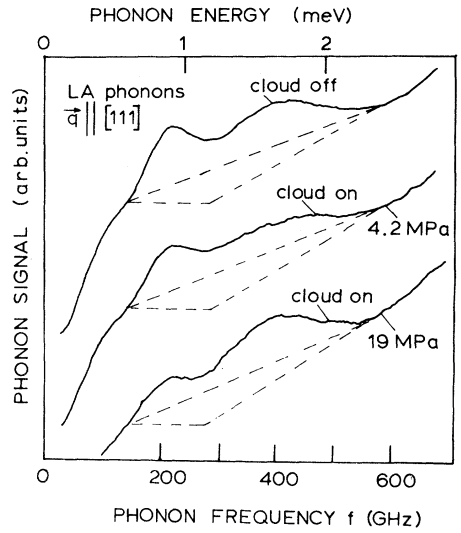

FIG. 13. Data showing the shift of the absorption maximum with stress. The top trace was with the laser blocked and remained unchanged with varying stress. The middle trace (4.2 MPa) shows absorption at all frequencies, whereas the bottom trace (19 MPa), when compared to the top trace, shows very little absorption above 350 GHz.

described above, we performed experiments with $\vec{q}||[110]$. The data in the [110] direction did not show a measurable absorption within our frequency range. This is consistent with the theoretical predictions because the $2k_F$ cutoffs in this direction are close to or below the detector-threshold frequency of 150 GHz.

Even though we could not observe the $2k_F$ cutoff in the [111] experiment by modifying the electron-hole liquid, it is possible to reduce the predicted $2k_F$ cutoff frequency below the onset of isotope scattering by applying stress in the $[11\bar{1}]$ direction, as discussed in Sec. II.

Phonon absorption measurements on stressed Ge were performed in the same way as the zero-stress experiments. We used a sample with a smaller cross section in order to reduce the force required for a given strain. The maximum cloud size was restricted by the smaller sample dimensions which led to a somewhat smaller phonon absorption. Also the isotope-scattering cutoff was at a slightly higher frequency in this sample because of the shorter phonon path length.

In Fig. 13 we show phonon spectra taken at two different stresses. The top trace was taken with the laser blocked. Without EHL the phonon spectra were found to be independent of stress. The second trace was taken at a moderate $[11\bar{1}]$ stress (4.2 MPa) and is similar to the "cloud-on" trace in Fig. 11. The absorption is strongest around 400 GHz. The third trace was taken at 19 MPa. At frequencies above about 350 GHz, it is very similar to the top trace (cloud off), but at lower frequencies there is still absorption due to the cloud.

We made the same quantitative analysis for the data at these and other stresses as we did for the zero-stress case. The resulting d/l plots are shown in Figs. 12(b)–12(e). The dashed lines are fits to the theory, again using the product $\Xi_\alpha^2 d$ as the only adjustable parameter. The experimental and theoretical frequency dependences are in reasonably good agreement at all stresses.

Together with the theoretical analysis, these data verify the basic phonon absorption model and demonstrate the existence of a $2k_F$ cutoff in the EHL. It should be noted that the theoretical curves do not require k_F as a fitted parameter: k_F is determined by the measured stress, the well-known conduction-band splitting, and the measured[21] Fermi energies at finite stress. In the next section we will estimate the effective liquid thickness d so that the magnitude of the absorption strength can be determined and compared with theory.

D. Density of the EHL cloud

The volume between generator and detector is not homogeneously filled with carriers. Instead, the droplet density is high near the excitation spot and falls off with increasing distance. If the laser is very well focused, the cloud shows a marked anisotropy[9] which is largely due to the phonon focusing properties of Ge. We avoided these features and optimized the number of droplets in the phonon path by slightly defocusing the laser.

The parameter d is the average path length which the phonon travels *inside* droplets. Experimental determination of d requires a knowledge of the filling factor and extent of the cloud, quantities which depend upon the particular experimental geometry and excitation conditions.

We used an infrared-imaging system[9] to determine the spatial distribution of the cloud. The absolute value of the cloud density was then inferred from a comparison of the luminescence intensity of the EHL cloud with that of a single large strain-confined drop of EHL, previously referred to in the literature as a γ drop.[31] The density of this large drop was established spectroscopically.[23]

The luminescence signal I_l measured with the imaging system is given by

$$I_l = SN/\tau_{ar} \ , \tag{5}$$

where the constant S reflects the sensitivity of the system, N is the total number of pairs sampled by crossed slits at the spectrometer entrance, and τ_{ar} is the radiative lifetime of EHL droplets at zero stress. Since the measured total lifetime of the EHL is 40 μsec and previous estimates[32] of a radiative efficiency are about 25%, this implies that $\tau_{ar} \approx 150$ μsec.

Figure 14 shows experimental scans (solid lines) of I_l across the crystal for two orthogonal viewing directions. The view along x contains a spurious contribution (the lump between 0.2 and 1.0 mm)

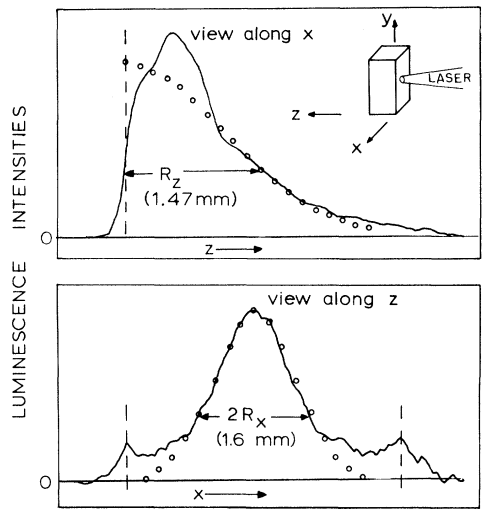

FIG. 14. Luminescence profiles of the EHL cloud for the x and z directions (see inset). The lump on the top trace is a reflection of luminescence light from one of the junctions. The dots are fits to Eq. (6).

which is a reflection of luminescence light from one of the tunnel junctions. To facilitate the analysis we assume that the average electron-hole pair density $n_{\rm av}(x,y,z)$ has a Gaussian distribution

$$n_{\rm av}(x,y,z) = n_0 \exp(-x^2/R_x^2 - y^2/R_y^2 - z^2/R_z^2) \ . \tag{6}$$

By integrating this function over the volume sampled by our spectrometer slits, we fit the resulting one-dimensional Gaussian function to our luminescence profiles. The measured R's were of order one millimeter, as shown.

The next step is to determine S, i.e., calibrate the imaging system. At higher stresses in our Ge crystals, large spherically shaped γ drops were formed adjacent to the blocks clamping the sample, due to stress inhomogeneities. In a γ drop at this crystal stress both density (0.5×10^{17} cm^{-3}) and radiative lifetime ($\tau_{\gamma r} = 700$ μsec) are reasonably well known.[23] We measured the diameter of the γ drop and its luminescence intensity and thus determined S for our system, assuming constant density inside the γ drop.

For the cloud produced in the phonon spectroscopy experiments of Figs. 10–12 we found $n_0 = 1.2\times10^{15}$ cm^{-3}, $R_x \approx R_y = 0.83$ mm, and $R_z = 1.47$ mm. The average cloud density determined in this way is very close to that measured by Voos *et al.* from infrared-laser absorption.[33] The total number of electron-hole pairs in the monochromatic phonon path is now obtained from integrating Eq. (6) along the phonon path. This

result is $N=2.5\times10^{12}$ pairs/cm^2. Dividing this number by 2.38×10^{17} cm^{-3}, the pair density within a drop, gives $d=11$ μm. We believe that this estimate is good within a factor of 2. The primary uncertainty arises from a lack of precise knowledge of the radiative lifetime of electron-hole droplets.

For the analysis of the stress data we accounted for the fact that $\tau_{\rm rad}$ changes with stress. We assumed that it increases in proportion to the inverse of the EHL density which is a reasonable approximation for our stresses.[21] We found d to be 6, 6, 7, and 11 μm for the stresses 4.2, 5.8, 9.7, and 19 MPa, respectively.

As previously mentioned, our analysis of the phonon absorption implies that the total phonon beam area is covered by droplets. If this were not the case, Eq. (4) would be modified to

$$I=I_0[C\exp(-d/l)+1-C]\ , \tag{7}$$

where C is the fractional coverage of the phonon beam by droplets. From statistical arguments C is given by

$$C=1-\exp(-\pi R_d^2 N_d/A)\ , \tag{8}$$

where R_d is the droplet radius and N_d the number of droplets in the phonon beam of area A. Since $N_d\propto R_d^{-3}$ (keeping the number of *pairs* in path constant) C is determined by R_d.

Light scattering has been used by several groups[34–36] to measure droplet radii. The values obtained near our temperature vary between 2 and 5 μm. This yields values of C between 0.95 and 0.70, respectively, for a measured N_d/A of about 2×10^7 cm^{-2}.

Our measurements of I/I_0 directly give a lower limit to the coverage factor C. The absorption of 450-GHz phonons by EHL is 75% of the incident flux, as shown in Fig. 12(a). This requires that $C\geq0.75$. However, the frequency dependence shows no indication of I/I_0 limiting at this value. (This saturation would be visible if the high absorption were due to a higher scattering probability and a lower coverage.) Since a saturation of I/I_0 is not observed, we conclude that C must be significantly larger than 0.75. In fact, for $C<0.90$ deviations from linearity in the prediction of Eq. (7) produce a much poorer fit to the data. Thus the coverage must be at least 0.90 for our experiments, which is consistent with our empirical estimates above for droplets of radii ~2 μm.

E. Deformation potential

Knowing d, it is straightforward to find the experimental values of the deformation potential from the theoretical fits of Fig. 12. A systematic error is introduced by the deviation of (6) from the real cloud shape. However, the Gaussian form fits the spatial profiles quite well and the integral along the phonon path will be relatively insensitive to the exact functional form of $n_{\rm av}$. The error in N due to a non-Gaussian cloud shape can be estimated from Fig. 14 to be less than 10%.

In the $\langle111\rangle$ directions the deformation potential for longitudinal phonons is

$$\Xi^2_{\langle111\rangle,l}=(\Xi_d+\Xi_u)^2\ .$$

From our data we find $\Xi^2_{\langle111\rangle,l}$ to be 15^{+15}_{-8} eV^2, where the error is due primarily to the systematic uncertainty in the EHL radiative lifetimes. Under 4.2, 5.8, 9.7, and 19 MPa we obtain 12, 15, 16, and 16 eV^2, respectively. Thus, there is no stress dependence within the statistical error.

Our value of the total deformation potential is approximately one third that of a cyclotron resonance measurement[15] of 49 eV^2 for free electrons. Markiewicz predicted[16] that screening should *increase* this value to 144 eV^2. This unexpected increase in the predicted interaction strength came about because only Ξ_d was screened—changing from Ξ_d (unscreened)$=-12.3$ eV to $\Xi_d=-7.3$ eV using Thomas-Fermi screening. However, the criterion for the validity of the Thomas-Fermi approximation is that the phonon wavelength is much longer than the screening length, or $q\ll\kappa_{\rm TF}$, which is not satisfied for EHL in Ge when $q\approx2k_F$. Specifically, for LA phonons along $\langle111\rangle$, $2k_F=6.46\times10^6$ cm^{-1} and $\kappa_{\rm TF}\approx5\times10^6$ cm^{-1}.

Using the more general random-phase approximation (RPA), Pan, Smith, and McGill[37] predicted a twofold *decrease* in the electron scattering rate from its unscreened value. This decrease in interaction strength is in qualitative agreement with our measurement of Ξ^2_α. The screened deformation potentials associated with the RPA calculation are not presently available.

The experimental Ξ^2_α is proportional to the ratio of the radiative lifetimes ($\tau_{\gamma r}/\tau_{\alpha r}$) of the EHL. In anticipation of a more precise measurement of $\tau_{\gamma r}/\tau_{\alpha r}$ we state our zero stress result in the following way as well: $\Xi^2_{\langle111\rangle,l}=(3.2\pm0.8)(\tau_{\gamma r}/\tau_{\alpha r})$ eV^2. The error here is due to the error in fitting the parameter $\Xi^2_\alpha d$ as well as noise and drift in the imaging system.

IV. DISCUSSION

The basic results of Fig. 11 can also be expressed in terms of a scattering (or absorption) time of the phonons in EHL. With our estimate of $d \approx 11$ μm from the EHL luminescence intensity, Fig. 13(a) shows that the mean free path l of phonons traveling through EHL varies between 20 μm at 170 GHz and 5 μm at 480 GHz at our experimental temperature $T = 1.3$ K. This would correspond to a phonon lifetime of $\tau = l/v_s \approx 4$ nsec at 170 GHz and 1 nsec at 480 GHz.

Our principal result is that the phonon mean free path has a frequency dependence which is consistent with deformation potential scattering of phonons by a Fermi liquid. The predicted $2k_F$ cutoff was observed and agrees quantitatively with that predicted for the electron-hole liquid. The observation of this cutoff relied upon our ability to deform the Fermi surface of the liquid with stress. We demonstrated experimentally that even though the EHL Fermi energy is rather weakly dependent on stress, the Fermi wave vector along certain $\langle 111 \rangle$ directions can be reduced by nearly a factor of 4. In a practical sense, measurement of the $2k_F$ cutoff provides a unique method for observing the depopulation of the up-shifted $\langle 111 \rangle$ valleys.[38]

A unique aspect of the spectroscopy experiments on EHL is that they measure the phonon deformation potential for a specific mode and wave vector. In principle, it should be possible to extend our measurements to other propagation directions and modes. Measurement of the TA-phonon absorption would allow a separate determination of the two deformation potential constants Ξ_u and Ξ_d. This would resolve the remaining details involving screening effects: Which term(s) is screened and by how much is the value(s) changed? The absorption of TA phonons is quite weak, however, and a method must be devised to increase the amount of liquid in the phonon path.

ACKNOWLEDGMENTS

The authors would like to thank M. Greenstein, G. A. Northrop, and M. A. Tamor for their constructive discussions and computer software. Also, we thank D. M. Ginsberg for the use of his evaporator, E. E. Haller and W. L. Hansen of Lawrence Berkeley Laboratory for the Ge crystals, and R. S. Markiewicz for his helpful correspondence. This research was supported in part by the National Science Foundation under The Materials Research Laboratory Grant No. DMR-80-20250. The infrared-imaging system was developed under the NSF Grant No. DMR-80-24000. Travel support for W. Dietsche was provided by the Deutsche Forschungsgemeinschaft. S. Kirch was supported by an Exxon Research Fellowship. Support for phonon spectroscopy equipment was provided in part by an A. O. Beckman Research Award.

APPENDIX: ISOTOPE SCATTERING

Natural Ge consists of a mixture of several isotopes. This variation in the masses of the atoms in the crystal causes a very effective scattering of high-frequency phonons. This scattering process was treated theoretically by Klemens[39] who derived the following expression for the phonon lifetime:

$$\tau_{\rm iso}^{-1} = A\omega^4 \tag{A1}$$

with

$$A = \frac{V_0}{4\pi v_s^3} \sum_i r_i \left[1 - \frac{M_i}{M} \right]^2 ,$$

where V_0 is the volume per atom, M_i and r_i are the mass and relative fraction of the isotope i, respectively, M is the average mass of all atoms, v_s is the average sound velocity, and $\omega = 2\pi f$ is the phonon frequency. The quantity A was calculated[40,41] for Ge to be 2.4×10^{-44} sec^3. It was observed that A does not depend on the phonon polarization.[42] In the case of Ge, the concept of the isotope scattering was studied experimentally by thermal-conductivity[41] and heat-pulse[42] experiments.

In our experiment, the isotope scattering imposes a high-frequency limit on the ballistic phonon propagation. This is demonstrated in Fig. 15, which

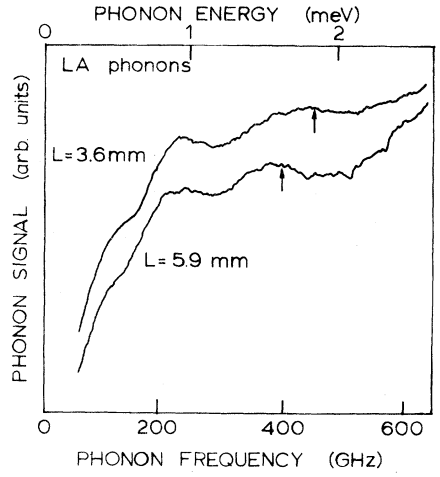

FIG. 15. Phonon spectra showing a reduction in the transmission of high-frequency phonons with increasing path length. The arrows indicate the frequency for which $L = v\tau_{\rm iso}$ with $\tau_{\rm iso}$ the scattering time predicted in Eq. (9).

shows phonon spectra of LA phonons obtained in two samples of different thicknesses without EHL clouds present. All traces show an intensity decrease above 350 to 450 GHz. The arrows mark the phonon frequency where the predicted mean free path due to isotope scattering, Eq. (A1), equals the distance from generator to detector (L). The agreement between these frequencies and the frequencies of the phonon intensity decrease is rather good. We conclude from these data that in Ge phonon scattering by different isotopes is very well described by theory.

---

*Present address: Physik Department, TU München, W. Germany.

[1]For a review see T. M. Rice, J. C. Hensel, G. A. Thomas, and T. G. Phillips, in *Solid State Physics,* edited by H. Ehrenreich, F. Seitz, and D. Turnbull (Academic, New York, 1977), Vol. 32.

[2]L. V. Keldysh, Zh. Eksp. Teor. Fiz. Pis'ma Red. 23, 100 (1976) [JETP Lett. 23, 86 (1976)].

[3]V. S. Bagaev, L. V. Keldysh, N. N. Sibel'din, and V. S. Tsvetkov, Zh. Eksp. Teor. Fiz. 70, 702 (1976) [Sov. Phys.—JETP 43, 362 (1976)].

[4]J. C. Hensel and R. C. Dynes, Phys. Rev. Lett. 39, 969 (1977).

[5]M. Greenstein and J. P. Wolfe, Phys. Rev. Lett. 41, 715 (1978).

[6]J. Doehler and J. M. Worlock, Phys. Rev. Lett. 41, 980 (1978).

[7]V. S. Bagaev, G. Bel'skaya-Levandovskaya, M. M. Bonch-Osmolovskii, T. I. Galkina, S. Y. Levandovskii, G. N. Mikhailova, A. G. Poyarkov, and G. Jung, Zh. Eksp. Teor. Fiz. 77, 2117 (1979) [Sov. Phys.—JETP 50, 1013 (1979)].

[8]R. S. Markiewicz, M. Greenstein, and J. P. Wolfe, Solid State Commun. 35, 339 (1978).

[9]M. Greenstein and J. P. Wolfe, Phys. Rev. B 24, 3318 (1981).

[10]D. Huet, B. Pannetier, F. R. Ladan, and J. P. Maneval, J. Phys. (Paris) 37, 521 (1976).

[11]H. Kinder, Phys. Rev. Lett. 28, 1564 (1972); Z. Phys. 262, 295 (1973).

[12]For a comprehensive review of this technique see W. Eisenmenger, in *Physical Acoustics,* edited by W. P. Mason (Academic, New York, 1976), pp. 79–153.

[13]J. Bardeen and W. Shockley, Phys. Rev. 80, 72 (1950).

[14]C. Herring and E. Vogt, Phys. Rev. 101, 944 (1956).

[15]K. Murase, K. Enjouji, and E. Otsuka, J. Phys. Soc. Jpn. 29, 1248 (1970).

[16]R. S. Markiewicz, Phys. Status Solidi B 83, 659 (1977).

[17]E. M. Conwell, *High Field Transport in Semiconductors,* Suppl. 9 of *Solid State Physics* (Academic, New York, 1967).

[18]T. M. Rice, Nuovo Cimento 23B, 226 (1974).

[19]V. I. Gavrilenko, V. L. Kononenko, T. S. Mandel'shtam, V. N. Murzin, and S. A. Saunin, Zh. Eksp. Teor. Fiz. Pis'ma Red. 26, 102 (1977) [JETP Lett. 26, 95 (1977)].

[20]C. Benoît à la Guillaime, M. Voos, and F. Salvan, Phys. Rev. B 5, 3079 (1972).

[21]H-h. Chou and G. K. Wong, Phys. Rev. Lett. 41, 1677 (1978).

[22]G. A. Thomas and Y. E. Pokrovskii, Phys. Rev. B 18, 864 (1978).

[23]J. P. Wolfe, R. S. Markiewicz, S. M. Kelso, J. E. Furneaux, and C. D. Jeffries, Phys. Rev. B 18, 1479 (1978).

[24]For a review of currently available techniques see, W. E. Bron, Rep. Prog. Phys. 43, 301 (1980), and references therein.

[25]R. J. von Gutfeld and A. H. Nethercot, Phys. Rev. Lett. 12, 641 (1964).

[26]H. Kinder and W. Dietsche, *Phonon Scattering in Solids,* edited by L. J. Challis, V. W. Rampton, and A. F. G. Wyatt (Plenum, New York, 1976), p. 199.

[27]W. Eisenmenger and A. H. Dayem, Phys. Rev. Lett. 18, 125 (1967).

[28]G. Northrop and J. P. Wolfe, Phys. Rev. B 22, 6196 (1980).

[29]V. S. Bagaev, T. I. Galkina, O. V. Gogolin, L. V. Keldysh, Zh. Eksp. Teor. Fiz. Pis'ma Red. 10, 309 (1969) [JETP Lett. 10, 195 (1969)].

[30]W. Zoller, W. Dietsche, H. Kinder, A. M. de Goër, and B. Salce, J. Phys. C 13, 3591 (1980).

[31]R. S. Markiewicz, J. P. Wolfe, and C. D. Jeffries, Phys. Rev. B 15, 1988 (1977).

[32]K. Betzler, B. G. Zhurkin, and A. L. Karuzskii, Solid State Commun. 17, 577 (1975).

[33]M. Voos, K. L. Shaklee, and J. M. Worlock, Phys. Rev. Lett. 33, 1161 (1974).

[34]Y. E. Pokrovskii and K. I. Suistonova, Zh. Eksp. Teor. Fiz. Pis'ma Red. 13, 297 (1971) [JETP Lett. 13, 212 (1971)].

[35]J. M. Worlock, T. C. Damen, K. L. Shaklee, and J. P. Gordon, Phys. Rev. Lett. 33, 771 (1974).

[36]V. S. Bagaev, N. V. Zamkovets, L. V. Keldysh, N. N. Sibeldin, and V. A. Tsvetkov, Zh. Eksp. Teor. Fiz. 70, 1501 (1976) [Sov. Phys.—JETP 43, 783 (1976)].

[37]D. S. Pan, D. L. Smith, and T. C. McGill, Phys. Rev. B 17, 3284 (1978).

[38]Electrons in these valleys have been termed, "hot electrons," and recent papers have examined the possibility of phase transitions between hot and cold EHL. See for example, J. Bayaj, F.-M. Tong, and G. K.

Wong, Phys. Rev. Lett. 46, 61 (1981).
[39]P. G. Klemens, Proc. Phys. Soc. London Sect. A 68, 1113 (1955).
[40]G. A. Slack, Phys. Rev. 105, 829 (1957).
[41]J. Callaway, Phys. Rev. 113, 1046 (1959).
[42]J. C. Hensel and R. C. Dynes, in *Phonon Scattering in Condensed Matter,* edited by H. J. Maris (Plenum, New York, 1980), pp. 395—400.

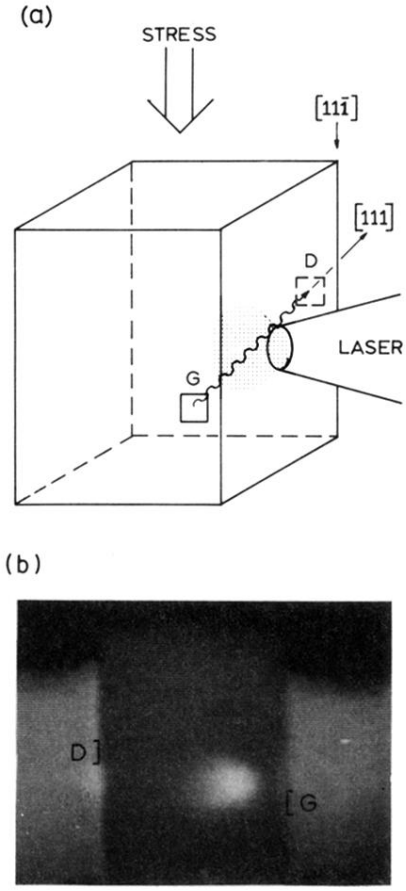

FIG. 9. (a) Schematic of the stressed crystal orientation. The generator (G) and detector (D) are on opposite faces of the crystal approximately 0.5 mm from one edge placed so that the phonons propagate in the desired direction [111]. A slightly defocused laser beam (spot size $\simeq$0.5 mm) produced a cloud of droplets which intercepted the phonon path. Stress was applied in the [11$\bar{1}$] direction corresponding to Fig. 7(b). (b) Photograph of an infrared vidicon image showing the actual crystal. The view is toward the laser. The bright spot is luminescence from the EHL cloud. The positions of the generator and detector are shown.